Geological Society of America
Special Paper 398
2006

Spatial patterns of precipitation and topography in the Himalaya

Alison M. Anders[†]
Gerard H. Roe
Bernard Hallet
David R. Montgomery
Noah J. Finnegan
Jaakko Putkonen
Earth and Space Sciences, University of Washington, P.O. Box 351310, Seattle, Washington 98195-1310, USA

ABSTRACT

Spatial variability in precipitation has received little attention in the study of connections between climate, erosion, and tectonics. However, long-term precipitation patterns show large variations over spatial scales of ~10 km and are strongly controlled by topography. We use precipitation rate estimates from Tropical Rainfall Measuring Mission (TRMM) satellite radar data to approximate annual precipitation over the Himalaya at a spatial resolution of 10 km. The resulting precipitation pattern shows gradients across the range, and from east to west along the range, and fivefold differences between major valleys and their adjacent ridges. Basin-wide average precipitation estimates correlate well with available measured mean runoff for Himalayan rivers. Estimated errors of 15%–50% in TRMM-derived annual precipitation are much smaller than the spatial variability in predicted totals across the study area. A simple model of orographic precipitation predicts a positive relationship between precipitation and two topographically derived factors: the saturation vapor pressure at the surface and this pressure times the slope. This model captures significant features of the pattern of precipitation, including the gradient across the range and the ridge-valley difference, but fails to predict the east-west gradient and the highest totals. Model results indicate that the spatial pattern of precipitation is strongly related to topography and therefore must co-evolve with the topography, and suggest that our model may be useful for investigation of the relationships among the coupled climate-erosion-tectonic system.

Keywords: orographic precipitation, remote sensing, Himalaya, landscape evolution.

INTRODUCTION

Growing evidence for a strong role of erosion in the tectonic and topographic development of mountain ranges motivates efforts to understand feedbacks between climate, erosion, and tectonics. While spatial gradients in erosional processes and tectonic forcing have prompted much study, most models of erosion consider climate to be spatially uniform. Yet spatial patterns in precipitation are influential both in shaping topography through erosion and as sensitive functions of topography at sub–mountain-range scales.

Spatial patterns of precipitation in Nepal (Barros et al., 2000), the Alps (Frei and Schär, 1998), and the Olympic Mountains (Anders et al., 2004; see also Barros and Lettenmaier, 1993) are characterized by remarkable and persistent variation on scales of tens of kilometers. Spatial variability in precipitation confounds the common substitution of drainage basin area for river discharge in modeling patterns of fluvial incision, and the use of this

[†]Present address: Department of Geology and Geophysics, Yale University, P.O. Box 208109, New Haven, Connecticut 06520-8109, USA; alison.anders@yale.edu.

Anders, A.M., Roe, G.H., Hallet, B., Montgomery, D.R., Finnegan, N.J., and Putkonen, J., 2006, Spatial patterns of precipitation and topography in the Himalaya, *in* Willett, S.D., Hovius, N., Brandon, M.T., and Fisher, D., eds., Tectonics, Climate, and Landscape Evolution: Geological Society of America Special Paper 398, p. 39–53, doi: 10.1130/2006.2398(03).

substitution in areas with strong spatial gradients in precipitation can lead to significant differences in predicted patterns of erosion (Roe et al., 2002, 2003; Finlayson and Montgomery, 2003).

Topography itself has a profound effect on spatial patterns of precipitation both globally and regionally (e.g., Smith, 1979). Mountains influence the flow of air and disturb the vertical stratification of the atmosphere by acting as physical barriers and as sources or sinks of heat (e.g., Barros and Lettenmaier, 1994). At the scale of entire mountain ranges (hundreds of km) the rain-shadow effect has a well-documented and significant influence on precipitation patterns. Enhanced precipitation on the windward side of mountain ranges has been recognized in the geological community as a long-term control on landscape evolution and the geotectonic development of mountain ranges (e.g., Koons, 1989; Beaumont et al., 1992; Hoffman and Grotzinger, 1993;Willett, 1999; Montgomery et al., 2001). However, forced ascent on the windward side is not the only way that the atmosphere interacts with topography; instead of rising over the topography, the air may be blocked or diverted around the range (e.g., Simpson, 1987). Alternately, the flow of air over the topography may excite internal waves, due to the vertical density stratification of the atmosphere (e.g., Durran, 1986). Mountains can also warm the air above them, drawing air from low levels up and triggering condensation or convection on the slopes, as has been observed in thunderstorms on the eastern slopes of the Rocky Mountains (Tripoli and Cotton, 1989). The vertical profiles of temperature and moisture content and the velocity of the incoming air, which vary from storm to storm, as well as characteristics of the topography, including the length, width, and height of the mountain range, determine how the atmosphere interacts with the mountains (e.g., Houze, 1993). Nevertheless, if spatial patterns of precipitation are relatively stable over time and are consistently related to topography in a given region, the pattern of erosion, and therefore the topography, must co-evolve with patterns of precipitation.

Current knowledge about the climatological annual precipitation pattern in the Himalaya is derived from rain gauges, and several interpolations are available (e.g., Leemans and Cramer, 1991, Shrestha, 2000). Additionally, basin-scale orographic precipitation patterns have been studied using rain gauges in the Chenab (Singh et al., 1995) and Kosi basins (Dhar and Rakhecha, 1981).

Orographic precipitation in a limited region of the central Himalaya has been documented with a dense gauge network and a variety of remote sensing techniques to investigate processes controlling precipitation distribution on the scale of 10–20 km during storm events and monsoon seasons (Barros et al., 2000; Lang and Barros, 2002, 2004; Barros and Lang, 2003). These studies have revealed large gradients in seasonal precipitation totals over short (~10 km) spatial scales that are not simply related to elevation (Barros and Lang, 2003). Additionally, they have documented differences in monsoon season (June–September) diurnal precipitation patterns at high (>2000 m) and low elevations that relate to daytime upslope winds switching to weak nighttime downslope winds (Barros et al., 2000; Barros and Lang, 2003). Satellite precipitation radar tracks reveal large regions of stratiform precipitation with embedded convective cells during the monsoon season (Lang and Barros, 2002). A spatial association of weak convective cells and clouds with SW facing ridges during the monsoon season was noted by Barros et al. (2004). Nearly all of the precipitation occurring below 2000 m is rain, while at higher elevation stations snow accounts for 17 ± 11% of annual precipitation totals, with this fraction increasing with elevation (Lang and Barros, 2004). Winter precipitation is associated with Western Disturbances that cause wintertime precipitation over northern India and Kashmir (Lang and Barros, 2004). See Barros et al. (this volume) for modeling studies of monsoon onset and winter storm events illustrating the role of complex topography in shaping cloud patterns.

The long-term pattern of precipitation in mountains generally and the Himalaya in particular is poorly constrained due to a lack of measurements of precipitation on spatial scales of a few tens of kilometers or less, and a lack of measurements extending back over more than a few years or decades. The dearth of information on spatial patterns of precipitation is in part due to the difficulty of measuring precipitation over appropriate spatial and temporal scales. Rain gauges provide information on precipitation, but existing rain-gauge networks, especially in mountainous areas, are generally not dense enough to reveal variability in precipitation over spatial scales of tens of kilometers—scales over which topography and precipitation can vary significantly. Rain gauges themselves are subject to several kinds of errors, including the local disturbance to flow that they create, the difficulty of automatically measuring snow water equivalence, and the fact that gauges are a point measurement and may not represent average precipitation over a larger region (e.g., Groisman and Legates, 1994; Sinclair et al., 1997; Dingman, 2002). In general, rain-gauge networks tend to undersample high elevations relative to lower elevations (e.g., Frei and Schär, 1998; Colle et al., 1999). The extrapolation from a rain-gauge network to a continuous field of precipitation via a statistical algorithm (such as the PRISM method of Daly et al., 2002) relies on an assumed relationship between precipitation and topography that is difficult to justify given the sparse sampling of gauge networks and space-time variability of weather conditions. Finally, the establishment and maintenance of dense gauge networks in remote mountainous regions such as the Himalaya is daunting and to date has only been done over one small area in the central Himalaya (Barros et al., 2000).

The remote sensing of precipitation via radar reflectivity, therefore, provides an attractive approach to defining spatial patterns of precipitation in mountains. The first spaceborne precipitation radar, aboard the Tropical Rainfall Monitoring Mission (TRMM) satellite provides a unique opportunity to assemble data on spatial patterns of precipitation in low-latitude mountain ranges. This instrument allows us, for the first time, to collect spatially continuous information on precipitation in mountains. As such, TRMM is a novel tool worth examining as a means

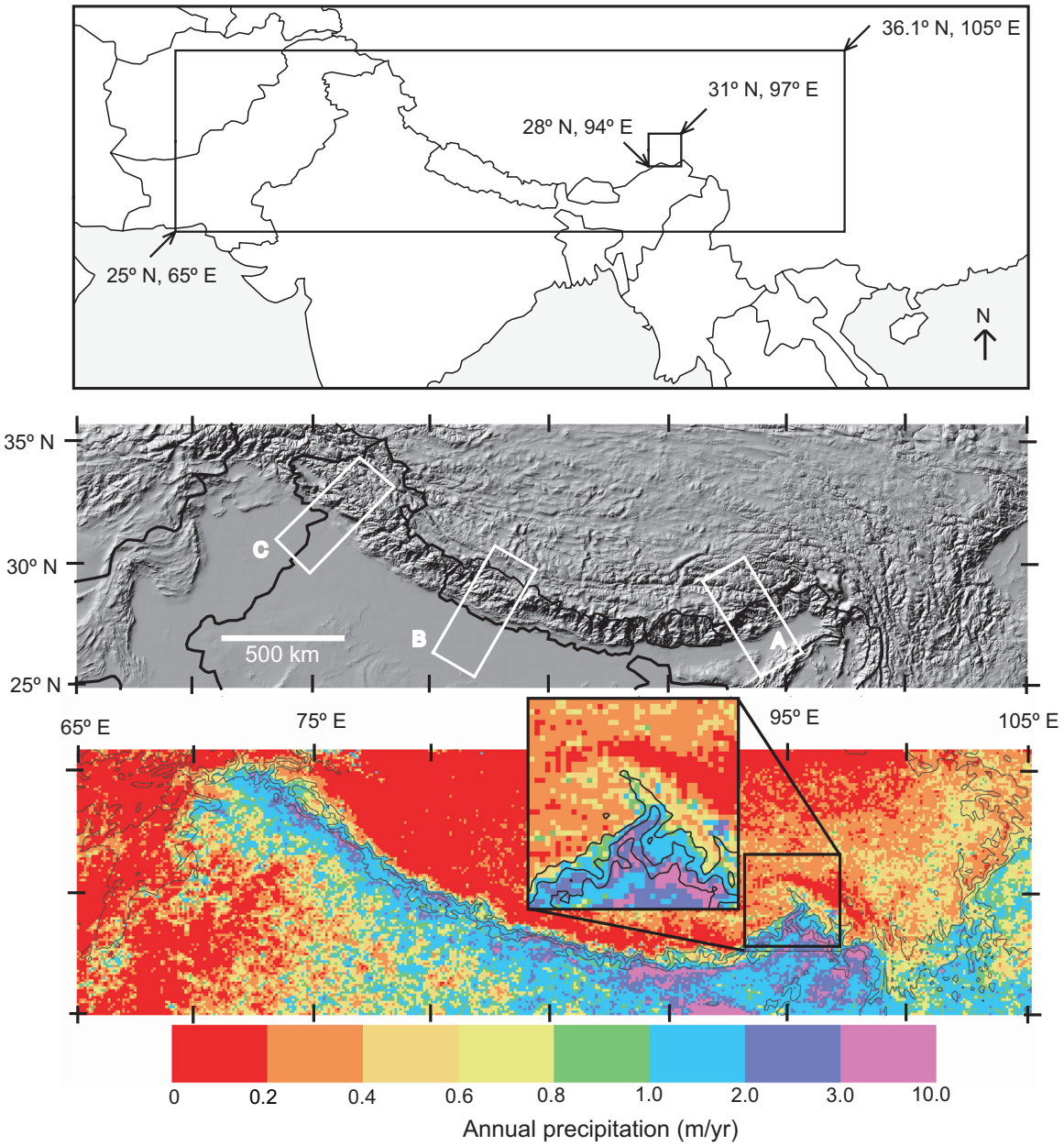

Figure 1. Location map, topography, and Tropical Rainfall Measuring Mission (TRMM) annual precipitation pattern. The study area is indicated in the top panel by the large box, along with a subregion near Namche Barwa at the eastern syntaxis of the range. The topography is shown in shaded relief in the middle panel, and the white boxes indicate the locations of cross sections shown in Figure 3. The lower panel shows the annual precipitation map (m/yr) that we created from four years of the TRMM satellite's precipitation radar precipitation rate estimates for the entire study area; inset is a close-up of the Namche Barwa region. The pattern of precipitation is closely related to topography. At the largest scale, the dry Tibetan Plateau and the wet Indian plains strongly contrast and a subtler gradient from east to west is apparent. At the scale of a few tens of kilometers, precipitation tracks topography, following large valleys north into the Himalaya. In addition, precipitation maxima in the southeastern end of the study area are observed with estimated annual precipitation totals in excess of 9 m/yr

of understanding spatial patterns of precipitation and erosion in areas sampled by the satellite. Herein, the focus is on using the TRMM satellite to define spatial patterns of annual precipitation in the Himalaya and to compare these patterns with topography in the context of geomorphological applications.

PRECIPITATION PATTERNS IN THE HIMALAYA FROM TRMM

The evaluation of landscape evolution–climate feedbacks in our study area requires a detailed map of precipitation rate

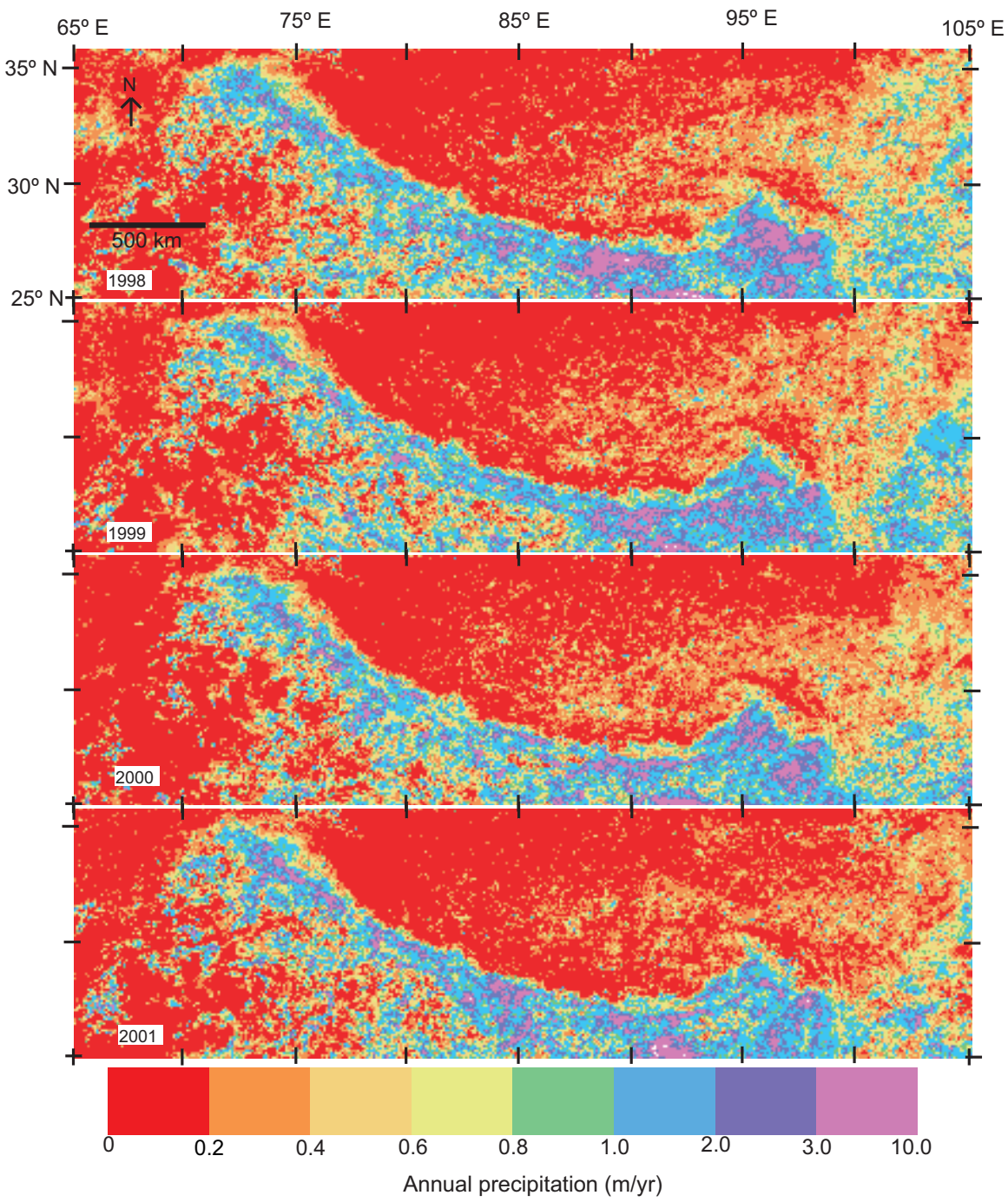

Figure 2. Four years of annual precipitation estimates from Tropical Rainfall Measuring Mission (TRMM). While there is some variability at the pixel scale (10 km), the overall pattern is remarkably consistent from year to year.

over a comparatively wide area (36°N–25°N, 105°E–65°E). The TRMM satellite uses spaceborne radar to provide accurate estimates of near-surface precipitation rates. We obtained the near-surface rain rate estimates from the 2A25 radar profile data (http://daac.gsfc.nasa.gov/hydrology/).

TRMM's precipitation radar operates at a frequency of 13.8GHz and can detect reflectivities down to ~18 dBZ, corresponding to rain rates of ~0.7 mm/h. Snow has a lower radar reflectivity for a given water equivalent than rain, and estimates of the relationship between reflectivity and water equivalent used

by the U.S. National Weather Service (http://www.nssl.noaa.gov/teams/watads/public_html/snow/snow.htm) suggest that the ~20 dBZ detection limit would still allow for detection of dry snow with > ~1 mm/h of water equivalent. However, the TRMM algorithms for converting measured reflectivity profiles to near-surface rain rates assume the precipitation is liquid water, which would underestimate the water-equivalence if the precipitation were snow. Additionally, the attenuation estimates are based on liquid precipitation rather than ice. The next generation of satellite precipitation measurement is being developed in the Global Precipitation Measuring Mission and may include a dual-frequency precipitation radar, which will be able to detect lower snow and rain rates and to distinguish between snow and rain using attenuation differences.

As discussed below in our estimates of sampling error, we must balance increasing spatial resolution against a decreasing number of instantaneous estimates of rain rate. This balance influenced our choice to grid our study area (Fig. 1) into 0.1 × 0.1 degree boxes (~10 km × 10 km).

TRMM provides 4 yr of instantaneous rain rate estimates in the study area (1998–2001), which are used to calculate the average rain rates and create a map of average annual precipitation (the climatology). The TRMM satellite orbit was designed to sample every location at different times of the day, over a 46 d cycle. By dividing each year of TRMM estimates into eight 46 d periods, an even sampling of the diurnal cycle was produced, and we avoided bias due to diurnal cycles in precipitation. The average rain rate for each 46 d period was multiplied by the duration of the period to get an estimated volume of precipitation for that time period. These volumes were then summed to obtain an annual precipitation total for each year (Fig. 2). The annual totals from each of the four years studied were averaged to create the average annual climatology (Fig. 1). The total number of samples in a grid box during a 46 d period varied from ~90 to ~400 as a function of latitude. About 95% of all samples were zeros (no precipitation). A small fraction (<0.01%) of the surface rain rate data exceeded 100 mm/h, which is unreasonable for regions larger than 100 km^2 (Kozu et al., 2001). These anomalous data values were considered artifacts and were removed from the analysis.

Figures 1 and 2 present the average annual precipitation climatology and the precipitation totals for each of the four individual years studied. This is the first time that spatially continuous precipitation data at such high spatial resolution (~10 km × 10 km) have been published for the Himalaya, and they reveal striking variability across, along, and within the range, as well as a robust spatial pattern that is consistent between all four individual years. The large-scale features of the precipitation pattern—namely the steep gradient in precipitation from the wet foreland to the arid Tibetan Plateau and the decrease in precipitation from east to west along the range—are clearly illustrated by the TRMM estimates (Fig. 3). In addition, there is remarkable structure at smaller scales, including large precipitation totals following big valleys up from the plains. This is illustrated in the inset portion

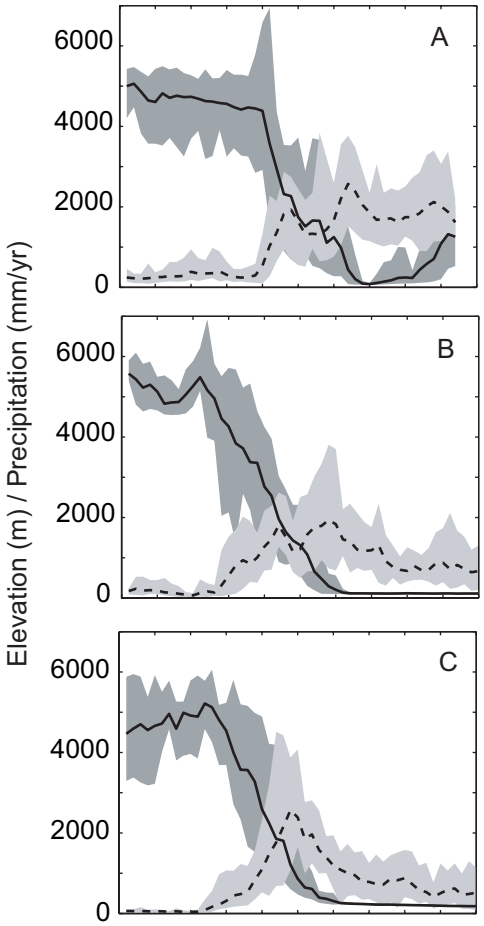

Figure 3. Cross sections of topography and precipitation. The black lines and dark gray shading show the mean elevation (m) and range of elevations along the cross sections indicated in Figure 1. The dashed line is the 4 yr average annual precipitation (mm/yr) estimated with Tropical Rainfall Measuring Mission (TRMM) precipitation radar. Light gray shading indicates the range of precipitation values. The correlation of precipitation and topography is evident in the sharp increase in both along the Himalayan front.

of Figure 1, which shows a subset of the data near the eastern syntaxis of the range. The zone of high precipitation closely follows the valley of the Tsangpo/Brahmaputra River north, as far north as regions that are within the dry higher Himalaya and southern Tibet, leading to large variations in precipitation between ridges and valleys along the strike of the range. In addition, a double band of high precipitation totals in the central and western portions of the range coincides with the first and second significant rises in topography approaching the Himalaya.

The stationary nature of the spatial pattern of annual precipitation in the four years studied is significant because it supports the notion that spatial patterns of precipitation are stable through time and hence would influence the evolution of topography through the related spatial pattern of erosion. The stability in time of relative differences in precipitation across space is a key

requirement for the co-evolution of precipitation patterns with topography. From the point of view of landscape evolution over timescales of 10^4–10^5 yr, we cannot necessarily constrain differences in the magnitude of precipitation in time due to long-term climate variability. But if the spatial pattern of relative precipitation totals is stable, the interactions among precipitation, erosion, and topography can be modeled.

ERROR ESTIMATION

Basin-Wide Average Annual TRMM Precipitation versus Measured Mean Annual Runoff

Evaluating the TRMM precipitation pattern with ground-based measurements is difficult, due to the general lack of rain gauges in the region. Barros et al. (2000) are currently working on the ground validation of the TRMM precipitation radar algorithm on an event basis in a small region in central Nepal. Herein, we wish to evaluate the TRMM-derived annual precipitation pattern at the drainage-basin scale, where data are available. Therefore, we turn to field measurements of river discharge, compiled from several sources by Finlayson et al. (2002) as a check on the integrated pattern of precipitation over drainage basins (Table 1, Fig. 4). The 19 basins were defined using digital topography from SRTM (Shuttle Radar Topography Mission) with a spatial resolution of 1 km. The average TRMM-derived precipitation within each basin was compared to the measured discharge in the basin divided by the basin area (annual mean runoff) (Fig. 4). There is a remarkable correlation

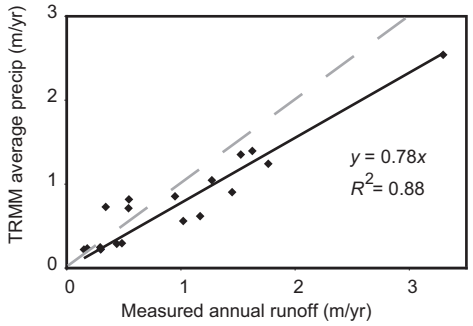

Figure 4. Tropical Rainfall Measuring Mission (TRMM) basin-wide average annual precipitation compared to measured mean runoff. The basin-wide averages of TRMM annual precipitation estimates correlate well with measured mean runoff (annual discharge/basin area) for 19 catchments listed in Table 1. The linear regression forced through the origin is shown as a black line. The 1:1 line is indicated by a dashed line. TRMM estimates generally fall below measured mean runoff values, suggesting that TRMM underestimates precipitation.

TABLE 1. RIVER DISCHARGE MEASURMENT LOCATIONS AND MEAN TROPICAL RAINFALL MEASURING MISSION (TRMM) ANNUAL PRECIPITATION

River and location	Latitude (°N)	Longitude (°E)	Basin area (km^2)	Measured discharge (km^3/yr)	TRMM average annual precipitation (m/yr)
Kali Gandaki—Koketani	84.4	27.8	3452	1.67	0.30
Kali Gandaki—Aval Beni	84.4	27.8	5637	5.35	0.85
Kali Gandaki—Ramdi	84.1	28.1	10,491	15.9	1.35
Kali Gandaki—Kot	84.5	27.9	44,819	19.20	1.40
Seti—Sarang Ghat	84.8	27.8	29,242	8.70	0.23
Seti—Kotre Bazar	84.9	27.8	997	3.29	2.54
Marsyandi—Markichok	85.2	28.0	4164	7.35	1.24
Bhuri—Beni Ghat	87.3	27.6	4994	6.35	1.05
Trisuli—Adamghat	87.2	27.3	5582	8.08	0.90
Trisuli—Betrawati	87.2	26.9	4640	4.73	0.56
Arun—606	74.4	36.0	57,705	19.70	0.73
Arun ?	74.6	35.6	31,268	13.70	0.29
Arun ?	72.9	34.8	29,941	8.92	0.22
Tsangpo—179	75.1	32.9	111,449	16.80	0.22
Tsangpo—180	74.4	34.3	170,793	30.70	0.23
Tsangpo—181	89.7	29.4	206,528	60.50	0.25
Jhelum—Baramula	92.0	29.3	12,380	6.70	0.71
Chenab—Alkhnoor	94.6	29.5	21,916	25.60	0.62
Chenab—Panjnab	84.4	27.8	181,226	98.60	0.82

between these quantities in a least-squares linear regression forced through the origin (TRMM average precipitation = 0.77 × measured unit discharge, $R^2 = 0.88$). This correlation is found for rivers with basin areas ranging from 1000–200,000 km^2, mainly along the Himalayan front. We recognize that the annual mean runoff of these rivers is influenced by evaporation and unreturned infiltration, which we do not attempt to model in addition to precipitation. However, the strong correlation between TRMM average precipitation and measured mean runoff indicates that TRMM-derived precipitation estimates provide a reasonable proxy for discharge along the Himalayan front and are an improvement over previous data sets, such as Leemans and Cramer (1991) used by Finlayson et al. (2002). Moreover, it suggests that the spatial pattern of precipitation estimated using TRMM is sufficiently well defined to capture the differences in average precipitation between these 19 basins for use in our purposes, namely, exploring the relationship between precipitation and topography and its role in long-term landscape evolution.

Ground Clutter Error Estimates

In addition to noting the empirical accord between TRMM average annual precipitation and measured mean runoff in a number of rivers, we also constrained the theoretical errors in using TRMM estimates to approximate annual precipitation totals. TRMM estimates are subject to both measurement error and sampling error. The former includes the error in the measurement of radar reflectivity, the attenuation correction to account for the decrease in reflectivity as the beam travels from the rain back to the satellite, and the semi-empirical rain rate–reflectivity relation. Efforts to estimate measurement errors are under way at various ground validation sites, including a site in Nepal that is included in our study area (Barros et al., 2000). A comparison of a limited data set of ~250–300 TRMM precipitation estimates (20–70 rain events) to gauge records at the Nepal calibration site shows a higher probability of detection with better skill scores as well as a higher false alarm rate for low elevation (<2000 m) versus high elevation gauges during the summer monsoon (Barros et al., 2000). This observation of bias at high elevations is not due to snowfall being missed, as these observations were made during the summer. Moreover, the same difference between high and low elevations is seen if only events with rain rates higher than 0.5 mm/h (theoretically within the sensitivity of the satellite) are considered (Barros et al., 2000). Part of this discrepancy could be related to the ground clutter algorithm truncating the profile above precipitation near the surface at high elevations.

As ground clutter artifacts could lead to a systematic, spatially coherent measurement error in mountainous regions, we investigated this component of the measurement error. Ground clutter artifacts are due to radar returns from Earth's surface that are misinterpreted as reflectivity due to water droplets. These commonly result from a radar beam reflecting off of steep slopes. As the incidence angle of the beam increases, the chance for slopes to reflect the beam increases. The ground clutter algorithm used in creating the TRMM near-surface rain rate field guards against ground clutter measurement errors by removing the data less than 1 km above the ground (Meneghini et al., 2000).

In the Himalaya, however, elevation can vary significantly over short spatial scales; several kilometers of relief are expected in some of our 100 km^2 grid boxes, complicating the removal of ground clutter artifacts. The algorithm may be too conservative and cut off reflectivity measurements from precipitation near the ground, or it may erroneously keep ground reflections from isolated peaks. To investigate the potential impact of ground clutter artifacts in the processed surface rain rates, we rely on the assumption that clutter is a function of incidence angle. Specifically, we examined near-surface rain rates as a function of look angle for a subregion of our study area near the eastern syntaxis of the Himalaya (29°N–31°N, 94°E–96°E). For the region as a whole, average rain rate is not a simple function of look angle (Fig. 5). However, the average rain rate over four years is slightly higher for look angles between 13.5 and 17 degrees (the highest look angles) than for look angles from 0 to 13.5 degrees (Fig. 5). This difference cannot be accounted for by either a few very large values of rain rate at high look angles, nor by a greater frequency of rain reported at high look angles. At high look angles, no rain is detected ~97% of the time, identical to that of the data set as a whole and to the subsamples with other look angles.

We examined the spatial pattern of average rain rate derived from samples taken at five classes of look angle and found that for the lowest four groups of look angle, the patterns are remarkably consistent. In the highest class of look angle, representing ~20% of the data, the pattern is somewhat different, with more precipitation measured in the high mountains to the northeast, suggesting some spatial coherence to the difference in rain rate between high and low look angles (Fig. 5). Further work could refine identification of the areas most influenced by this effect and evaluate the total impact on the error of removing the highest look angles from the data set. Nonetheless, for the purposes of this analysis, effects from ground clutter are small compared to the overall pattern, that is, the spatial pattern observed is not dominated by ground clutter artifacts. For the purpose of estimating annual discharge for use in landscape evolution modeling, ground clutter artifacts are negligible.

Sampling Error Estimates

The second type of error, sampling error, is the error in using a discrete number of measurements of rain rate to estimate the average rain rate and compute rainfall totals. When dealing with a small number of samples, sampling error is likely to be much larger than measurement error (Bell and Kundu, 2000). One of the goals of the TRMM mission is to produce monthly precipitation totals in 2° × 2° grids (approx. 40,000 km^2) over the area surveyed by the satellite. Several authors have concluded that these totals have sampling errors of ~10% (e.g., Shin and

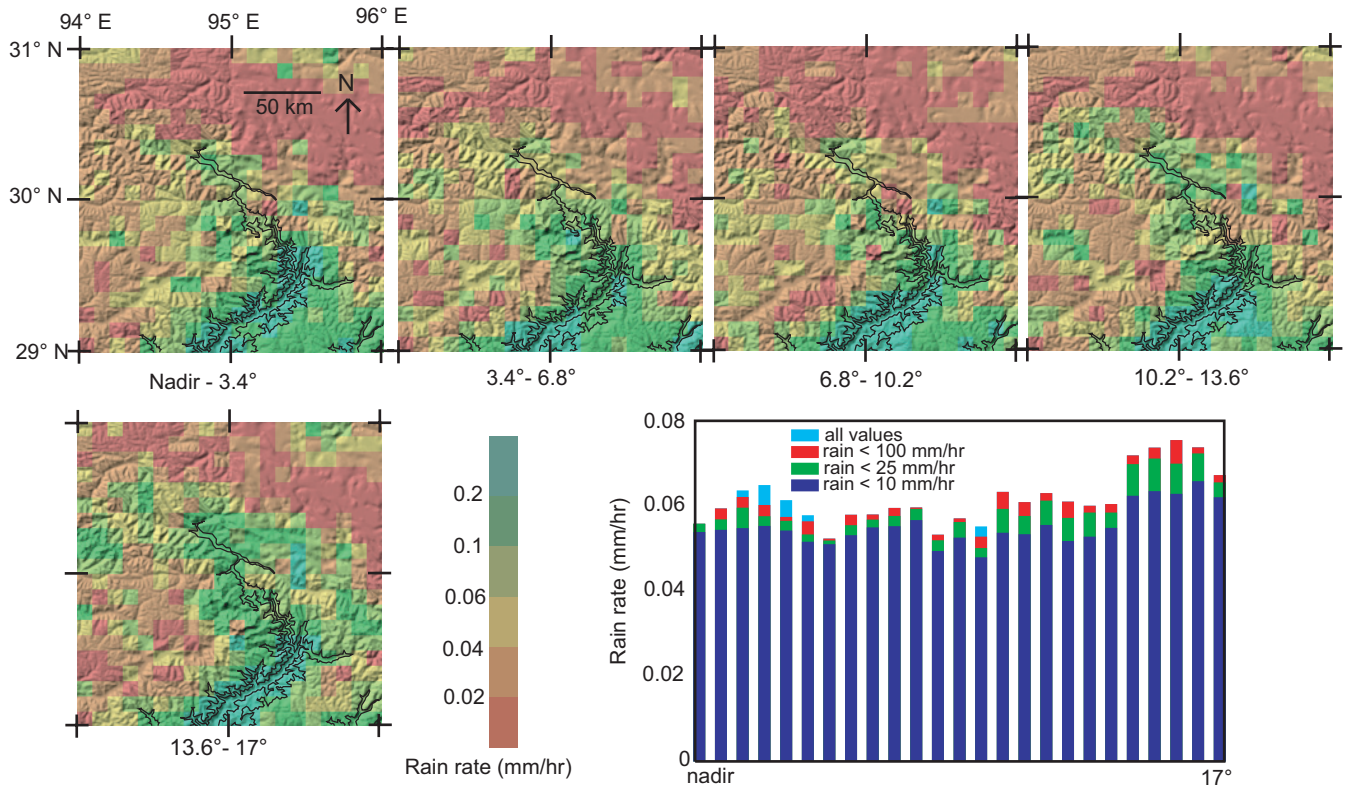

Figure 5. Rain rate as a function of look angle for the Namche Barwa region. The spatial pattern of average rain rate (mm/hr) over the Namche Barwa region is shown as a function of satellite look angle in 5 equal classes from 0 to 17 degrees. For the lowest four classes of look angle, the spatial pattern of rain rate is similar. However, for the highest look angles, higher rain rates are observed up the slopes to the northeast of the river valley than in the other classes, perhaps due to increased ground clutter errors at high look angles. In the lower right, the average rain rate over the Namche Barwa area is shown as a function of look angle, with various cutoffs in the largest values shown as different colors. The cutoff values are in mm/yr and range from 10 to no cutoff. Average rain rate over the domain is not a simple function of look angle, nor do large values of rain rate strongly influence the observed average rain rates.

North, 1988; Bell and Kundu, 2000). We used three independent methods to estimate the sampling errors we would expect for our much higher spatial resolution (100 km^2) precipitation totals with temporal resolution of 4 months to 1 yr (Table 2).

First, two rain-gauge precipitation records from the TRMM ground validation site in Nepal (Khudi, elevation 780 m, Koprung, elev. 3133 m; Barros et al., 2000) were used in a Monte Carlo simulation of sampling error. The year or monsoon-length rain-gauge record was randomly scrambled in day-length intervals and then sampled according to the TRMM overpass cycle to create 100,000 simulated TRMM records. The resulting simulated TRMM estimates of yearly and monsoon precipitation totals were compared to the gauge measurements over these periods to determine the error (standard deviation of the simulated TRMM samples divided by the total gauge-measured precipitation). The error determined from these simulations is 24%–30% for the year and 27%–29% for the monsoon season only (Table 2).

Shin and North (1988) and Bell and Kundu (2000) provided theoretical equations for satellite sampling error, both of which use a Markov model of precipitation such that:

$$R(\tau) = Be^{-|\tau|/\tau_0}, \quad (1)$$

where R is precipitation rate, τ is time, τ_0 is decorrelation time, and B is a constant. Shin and North (1988) proposed an equation based on the orbital parameters of the satellite as well as the decorrelation time of the precipitation and the coefficient of variation, defined as the constant B over the mean rain rate. We used three estimates of the decorrelation time, one of 1.1 h from Bell (1987), a maximum estimate of 10 h from Shin and North (1988), and estimates of 6 h and 5.7 h derived from fitting a Markov model to the Khudi and Koprung gauges in Nepal. We estimated the coefficient of variation using GATE (Global Atmospheric Research program Atlantic Tropical Experiment) data presented in Shin and North (1988), as well as their maximum estimate and one estimate calculated from the Nepal data. This range of parameters gave us nine estimates of yearly and monsoonal sampling error in precipitation totals of 14%–34% and 24%–60%, respectively (Table 1).

Bell and Kundu (2000) provided an alternate model of sampling error. We assume that our sampling grid resolution of

TABLE 2. SAMPLING ERROR ESTIMATES

Monte Carlo simulation			Annual 24%		Monsoon 27%	
Shin and North (1988) Estimate						
Decorrelation time (hrs)	1.1 Bell (1987) estimate		6 Nepal data estimate		10 Shin and North (1988) maximum estimate	
	Annual	Monsoon	Annual	Monsoon	Annual	Monsoon
CV = 5 estimate from GATE data	17%	30%	15%	27%	14%	24%
CV = 6.5 estimate from Nepal data	22%	39%	20%	35%	30%	32%
CV = 10 maximum estimate Shin and North (1988)	34%	60%	18%	54%	27%	49%
Bell and Kundu (2000) with rain rate estimate from Nepal						
Decorrelation time (hrs)	1.1 Bell(1987) estimate		6 Nepal data estimate		10 Maximum estimate Shin and North(1988)	
	Annual	Monsoon	Annual	Monsoon	Annual	Monsoon
	58%	52%	41%	37%	18%	17%

~10 km × 10 km is small enough that the entire area is receiving precipitation at the same time, so that Bell and Kundu's (2000) model reduces to

$$\varepsilon = \frac{r}{R}\left(\frac{1}{N} - \frac{2\tau_0}{T}\right)^{1/2}, \quad (2)$$

where ε is the sampling error, R is the average rain rate, r is the average rain rate while it is raining, N is the number of samples taken, T is the length of time over which the samples are taken, and τ_0 is the decorrelation time. Using the above-mentioned bounds on decorrelation time and using average rain rate and conditional rain rate from the Nepal data, this method yields error estimates of 18%–58% for yearly totals and 17%–52% for monsoon totals (Table 2).

Given the error estimates determined via the above three methods, we conclude that, even at 10 km resolution, sampling errors are small enough that the precipitation totals are suitable for the purposes we intend of estimating annual river discharge, modeling erosion, and comparing precipitation and topography throughout the Himalaya. At smaller spatial scales, the number of independent samples of precipitation rate decreases, making the errors greater according to all estimates. Therefore, the observed patterns can be used, albeit with caution, to investigate relationships between precipitation patterns and topography at spatial scales of 10 km and larger.

COMPARING PRECIPITATION AND TOPOGRAPHY

In addition to using observed precipitation fields to estimate modern fluvial incision rates, we are interested in understanding how topography and precipitation patterns co-evolve over long time periods. In order to address this question, models of how precipitation relates to topography are needed to determine how precipitation patterns change as topography evolves. Toward this end, we examine the relationship between the TRMM precipitation estimates and characteristics of the modern topography, including elevation and slope. While we note that precipitation patterns can be influenced by topography through many different mechanisms that depend on both topography and the conditions of the air upwind of the mountains, we evaluate a simple theoretical model of orographic precipitation using the observed patterns of precipitation and topography in the Himalaya. The degree to which a simple model is successful in producing a reasonable precipitation pattern gives an indication as to the potential for modeling the co-evolution of precipitation and topography with such a model.

Theoretical Model of Orographic Precipitation

Roe et al. (2002) propose a simple model of orographic precipitation in which precipitation is proportional to the vertically averaged convergence of the moisture flux plus a background term. This model incorporates two effects: the decrease in water vapor with height in the air column, and the change in temperature of the air as it is forced up the topography in the direction of the prevailing winds. Following Roe et al. (2002), the model assumes that orographic precipitation is proportional to two terms. The first is saturation vapor pressure at the surface, which is approximately proportional to the total column moisture content. The second factor is the saturation vapor pressure multiplied by the slope of the topography in the direction of the prevailing wind. Thus:

$$P \propto (\alpha + \beta \times S) \times e_{sat}(T), \quad (3)$$

where P is precipitation, S is slope in the direction of the wind, e_{sat} is saturation vapor pressure, T is surface temperature, and α and β are constants. The two factors in this model favor precipitation at low elevations and in areas with steep slopes facing into the dominant wind at low elevations. We denote surface saturation vapor pressure as *V*p and slope times saturation vapor pressure as *Sv*p.

In order to evaluate the fit of this model to the observations of precipitation and topography in the Himalaya, we must estimate the values of the two terms using the topography. First, the topographic data from GTOPO30 were smoothed to the resolution of the TRMM precipitation estimates (10 km × 10 km cells). We derived a representative surface saturation vapor pressure in each cell by first roughly estimating the air temperature using an average temperature of 30 °C at sea level and a constant lapse rate of 7 °C/km. The saturation vapor pressure (e_{sat}) as a function of temperature can be found using an approximation to the Clausius-Calpeyron relation:

$$e_{sat} = 6.112(mb)s^{\frac{17.67\Gamma}{243.5+T}}, \quad (4)$$

where T is temperature in degrees Celsius (e.g., Emanuel, 1994). This gives *V*p as a function of only elevation in the study area. To keep the model very simple, we compute *Sv*p by multiplying *V*p by the slope of the smoothed digital elevation model (DEM) in each grid box, neglecting the direction of the prevailing wind. Aspect could be introduced to this term as a proxy for wind direction. However, in the smoothed DEM of the Himalaya, the majority of steep slopes face the Indian side of the Himalayan arc, which is also the general direction of approach of the major weather systems (i.e., the mesoscale convective systems associated with the summer monsoons), suggesting that the addition of aspect into the model might be a relatively minor refinement. We compared these two topographic variables (*V*p and *Sv*p), as well as other simple topographic variables to the TRMM precipitation estimates using a statistical spatial regression model.

Statistical Relationships between TRMM Precipitation and Topographic Variables

The TRMM precipitation estimates, as well as the topographic variables, are autocorrelated in space; measurements for areas close together in space are likely to be close in value. Thus measurements at different locations are not strictly independent, and a simple regression model may overstate relationships between the variables. Therefore, we used a regression model that accounts for spatial lags of the variables (e.g., Anselin, 1993). It compares the values of chosen topographic variables at each point and the values of these variables at neighboring points to the local measured TRMM precipitation estimate. We used a MATLAB spatial statistics code (Pace and Barry, 1999) to find the ordinary least-squares (OLS) best-fit model of the form above and to evaluate the significance of each variable in this fit.

This model was used to find the best-fit coefficients for our theoretical model of orographic precipitation given the TRMM estimates and GTOPO30 topography. Additionally, we used the spatial regression technique for other topographic variables that may reasonably be related to precipitation, namely, slope (*S*), elevation relative to a reference elevation of 10 km (*E*), and the product of *S* and *E* (*Se*) to compare the fit for these variables versus that for our theoretical model. *E* is used rather than elevation relative to sea level, so that large values of *E* correspond to low elevations, as in *V*p, where large values are found at low elevations. These variables were chosen because they allow for the evaluation of the importance of the nonlinear relationship between *V*p and elevation versus the linear relationship between *E* and elevation, as well as the separation of the effects of slope alone in *S* and slope modified by an elevation term in *Sv*p and *Se*. All the variables were standardized [(value – mean)/standard deviation], as were the TRMM estimates, so that the units and absolute magnitudes of these variables would not be important to the analysis.

The statistical model accounts for the spatial autocorrelation of the topographic variables by computing an average of those variables at the four neighboring points for each point in the domain using a spatial weights matrix *W*. The observed values are regressed on both the topographic variables and the averages of the values at neighboring points (spatial lags). The *m* topographic ($t_1, t_2, \ldots t_m$) variables being evaluated are put into a matrix, T ($n \times m$):

$$T = \begin{vmatrix} t_1(1) & t_2(1) & \cdots & t_m(1) \\ t_1(2) & t_2(2) & \cdots & t_m(2) \\ \cdots & \cdots & \cdots & \cdots \\ t_1(n) & t_2(n) & \cdots & t_m(n) \end{vmatrix}. \quad (5)$$

The regression model takes the form:

$$T * \begin{vmatrix} a_1 \\ a_2 \\ \cdots \\ a_m \end{vmatrix} + W * T * \begin{vmatrix} b_1 \\ b_2 \\ \cdots \\ b_m \end{vmatrix} = TRMM + error, \quad (6)$$

where TRMM is the $n \times 1$ vector of the TRMM observations over the Himalaya, error is an $n \times 1$ vector of the difference between the estimate and the TRMM value, and the coefficients $a_1 - a_m$ are the OLS coefficients for the topographic variables, while $b_1 - b_m$ are the OLS coefficients for the spatial lags of those variables. We used the MATLAB code to compute the OLS estimates of the model parameters and the likelihood estimates for a hypothesis that each variable and its spatial lag have no effect.

The theoretical model of orographic precipitation that we present in equation 3 yields a good fit to the data in the spatial regression model with a mean error of 0.387. The model is shown in Figure 6 in the same units as the TRMM measurements (m/yr). Additionally, we examined the models that resulted from using every combination of 1–5 of the reasonable topographic vari-

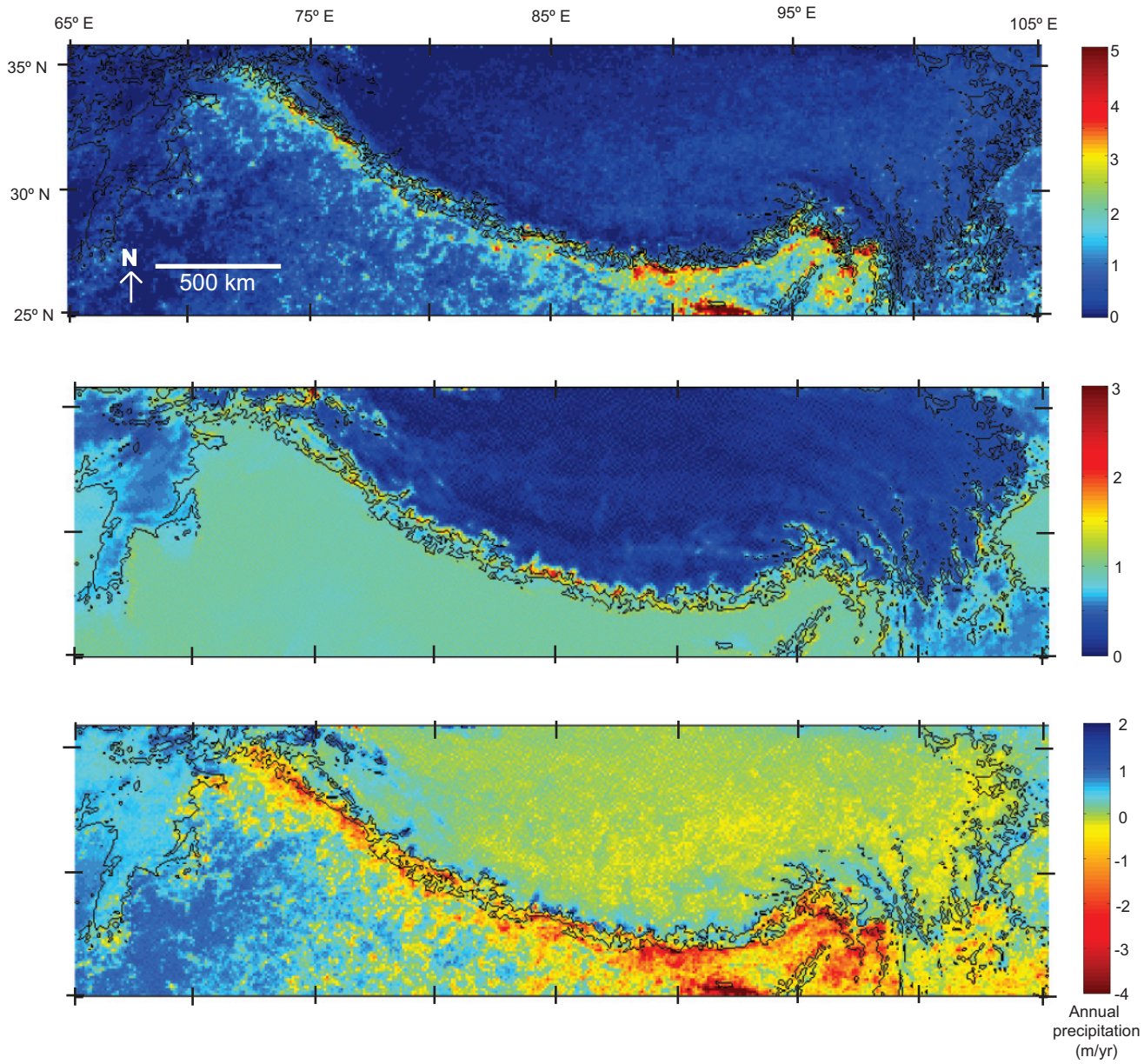

Figure 6. Tropical Rainfall Measuring Mission (TRMM) precipitation pattern, statistical model of precipitation, and error in the model. The TRMM-derived pattern of annual precipitation (m/yr) is shown over the entire study area in the top panel. The ordinary least-squares (OLS) best-fit model of this pattern using *V*p and *Sv*p, shown in the middle panel, captures the gradient across the range and the tracking of precipitation up major valleys. The error in the model in the lower panel, also in m/yr, shows that the large-scale east to west gradient, as well as the smaller-scale maxima in precipitation in the east, are not captured by the model. The solid lines indicate the 1500 and 3500 m topographic contours.

ables we considered (*V*p, *Sv*p, *S*, *E*, *Se*) and computed for each the mean absolute error and standard deviation of the error for each model. The errors from each model are given in Table 2.

Considering the best models with each number of variables, we find that *V*p is the best 1-parameter model with a mean error of 0.460. The best 2-parameter model is our favored theoretical model: *V*p and *Sv*p, with a mean error of 0.387. In examining the best models with more than 2 parameters, we find that the mean error is not substantially decreased by adding more parameters (0.367 for the best 3-parameter model, 0.360 for a 4-parameter model, and 0.356 for the 5-prarmeter model) (Table 3). The coefficients associated with the 3, 4, and 5 parameter models are difficult to interpret physically, as they include opposite signs for the coefficients of a variable and the spatial lags of the variable. The relative insensitivity of the mean error to the additional parameters, as well as the un-physical coefficients of these 3-, 4-, and 5-parameter models, indicates that the simpler, physically based, theoretical model not only is a good fit to the data, but also

TABLE 3. ERROR IN STATISTICAL MODELS

Variables	Mean absolute error	Standard deviation of the error
E	0.594	0.923
Vp†	0.460	0.806
S	0.716	0.995
Se	0.682	0.955
Svp	0.563	0.837
E, *Vp*	0.461	0.806
E, *S*	0.598	0.868
E, *Se*	0.573	0.836
E, *Svp*	0.487	0.751
Vp, *S*	0.458	0.759
Vp, *Se*	0.431	0.712
Vp, *Svp*†	0.384	0.666
S, *Se*	0.565	0.834
S, *Svp*	0.499	0.759
Se, *Svp*	0.516	0.769
E, *Vp*, *S*,	0.452	0.748
E, *Vp*, *Se*	0.424	0.707
E, *Vp*, *Svp*	0.347	0.664
E, *S*, *Se*	0.536	0.813
E, *S*, *Svp*	0.463	0.736
E, *Se*, *Svp*	0.459	0.730
Vp, *S*, *Se*	0.388	0.676
Vp, *S*, *Svp*†	0.367	0.658
Vp, *Se*, *Svp*	0.377	0.663
S, *Se*, *Svp*	0.499	0.759
E, *Vp*, *S*, *Se*	0.386	0.671
E, *Vp*, *S*, *Svp*	0.367	0.658
E, *Vp*, *Se*, *Svp*	0.374	0.661
E, *S*, *Se*, *Svp*	0.460	0.729
Vp, *S*, *Se*, *Svp*†	0.360	0.656
E, *Vp*, *S*, *Se*, *Svp*†	0.356	0.656

†The best model with each number of variables.

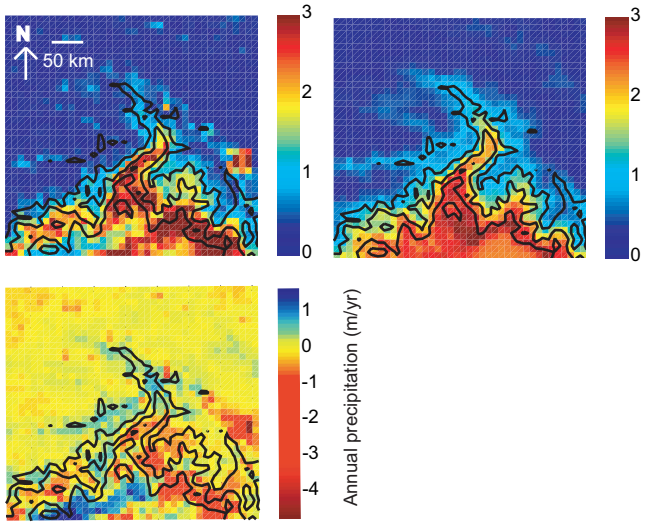

Figure 7. Model of Tropical Rainfall Measuring Mission (TRMM) data for the Namche Barwa subregion. The top left panel shows the TRMM annual precipitation estimates (m/yr). The top right panel shows the ordinary least-squares (OLS) model using *V*p and *Svp*. The error (model-data) is shown in the bottom panel. As in the case of the entire study area, the model describes principal elements of the precipitation pattern, but misses small-scale (<100 km) details. The solid lines indicate the 1500, 2500, and 3500 m topographic contours.

provides the best explanation of the observed pattern using the topographic variables we considered.

The coefficients for the OLS best-fit model with the parameters *V*p and *Svp* are 0.402 and 0.041 on *V*p and *Svp*, respectively, and 0.114 and 0.452 on their respective spatial lags. The model successfully captures some principal features of the TRMM precipitation pattern, including the dry plateau and the wet foreland at the large scale, and the wet valleys and dry ridges, as well as the double band of precipitation along the central front part of the range. However, as shown in Figure 6, the model fails to capture the extremely high values of precipitation in the eastern end of the range, largely fails to capture the gradient from east to west along the range, and predicts much smaller maximum precipitation totals (~3 m/yr versus 9 m/yr in the TRMM estimates).

In addition to the model for the whole Himalaya, the OLS best-fit coefficients for the preferred model were also found for a small subregion near the eastern syntaxis (Fig. 7); they are 0.014 and 0.216 for *V*p and *Svp*, respectively, and 0.509 and 0.227 on their spatial lags. As in the case above, the subregion model does capture principal aspects of the variability; the strong valley-ridge difference between the Tsangpo River and the surrounding high areas is reproduced in the model. Also, similar to the larger case, the model does not predict the largest precipitation totals in the TRMM estimates (~3.5 m/yr versus 6 m/yr). That the coefficients for this region differ so much from those for the whole study area is likely due to the greater importance of slopes on a regional scale; steep slopes comprise a greater fraction of small region than in the study area as a whole. It also reflects an inherent issue in modeling precipitation: processes involved in orographic precipitation are scale-dependent, and no single set of coefficients should be expected to be generally applicable.

DISCUSSION

The spatial pattern of precipitation as estimated from TRMM in the Himalaya shows considerable variability on scales less than 100 km—spatial variability that is repeated in four separate years of measurements (Figs. 1–3). Similar seasonal gradients are seen in gauge records from the calibration site in Nepal (Barros et al., 2000; Barros and Lang, 2003). Robust gradients in precipitation over spatial scales of tens of kilometers have important implications for both the study of orographic precipitation and for landscape evolution modeling. The fact that the large-scale pattern of precipitation does not change appreciably over time suggests that, at this scale, the pattern strongly reflects topography itself. Topography is obviously constant on this time scale, whereas the characteristics of the incoming air may vary significantly from event to event. At the pixel scale (10 km × 10 km) there are some large interannual differences; we cannot distinguish between those caused by sampling error and those by genuine variation in precipitation from year to year.

Large differences in annual precipitation occurring in areas only tens of kilometers apart along the strike of the mountain range show that the common use of uniform precipitation fields in landscape evolution models does not realistically depict within-range variability in the climatic influence on erosion, even at small spatial scales. Most importantly for the consideration of coupled climatic, erosional, and tectonic processes, the pattern of precipitation in the Himalaya is strongly controlled by the topography, as suggested by the success of our simple theoretical model and supported by remote sensing and modeling of cloud patterns in central Nepal (Barros et al., 2004). A pattern of precipitation that is robust and strongly related to topography must evolve as the topography develops and, hence, must also influence the development of topography through erosion. The co-evolution of precipitation patterns and topography merits further research.

The TRMM precipitation radar is a useful tool for studying precipitation and river discharge patterns in the Himalaya. TRMM can provide reasonable estimates of annual discharge for basins of more than 1000 km^2 in the Himalaya. However, TRMM estimates of average annual precipitation are consistently smaller than measured unit discharge (86% of measured unit discharge) (Fig. 4). Moreover, since they do not account for evapo-transpiration, we would expect that the TRMM estimates for the annual average precipitation in a basin would exceed annual unit discharge. TRMM radar does not detect very low precipitation rates (less than 0.7 mm/h), so, to the extent that events characterized by such precipitation rates contribute to annual total precipitation, TRMM will underestimate this total. Additionally, TRMM's 18 dBZ detection limit does not allow for observation of low-moderate snowfall rates and will underestimate the water equivalence of any snow detected. Snowfall is limited to higher elevations, and there is a tendency for more persistent and lighter rainfall at these same elevations at the Nepal calibration site (Lang and Barros, 2002, 2004). This suggests a bias toward underestimating precipitation at higher elevations. A comparison of TRMM precipitation estimates and measured mean runoff in other regions, especially those with known spatially varying average rain rates, could help constrain the errors associated with TRMM precipitation estimates at high elevations and in complex terrain.

In the Himalaya, ground clutter may have a subtle influence on measurements for look angles greater than 13.5 degrees, but does not greatly impact the observed pattern of TRMM precipitation estimates (Fig. 5). This influence is not seen in more observations of rain at high look angles than at lower look angles, nor as the addition of very high values of rain rate. Rather, the influence seems to be spatially correlated patches with higher average rain rates (Fig. 5). Our preliminary work suggests that a more extensive study of this problem could determine if the combination of measurement and sampling error would be improved by discarding the high look angle measures in some regions.

Three methods of constraining satellite sampling error suggest that for yearly and monsoon precipitation totals in the Himalaya, sampling errors of 15%–50% are likely (Table 2). These errors are not trivial, but neither are they so large as to overwhelm the observed spatial pattern of precipitation; annual precipitation in our climatology varies from a few tenths of a meter to nearly 10 m across the study area. The variability we measured spans nearly two orders of magnitude, far greater than the estimated 15%–50% error. The close correlation of basin-averaged annual precipitation estimates and measured mean runoff supports this conclusion. Moreover, we are primarily interested in the spatial variability in precipitation rather than the magnitude itself, in part because the interannual and longer time-scale variability in this region is largely unconstrained. Provided that spatial patterns similar to those we observed persist over geologically significant time scales, they will be important for questions of landscape (and possibly tectonic) evolution in the mountain range. Such patterns may persist despite changes in the magnitude of precipitation on the whole. Hence, the error estimates and correlation with discharge indicate that TRMM precipitation estimates can be used as a proxy for spatial patterns in precipitation in geomorphic applications, including discharge estimates for use in fluvial incision models and for evaluation of models of precipitation based on topographic variables.

The measurement and sampling errors involved in TRMM estimates of precipitation reported herein are likely to be dependent on conditions specific to the Himalaya. Ground clutter errors may be a function of the relief in the region and formal sampling error estimates require local parameters such as decorrelation time and average rain rate. Consequently, extension of this method of studying spatial patterns of precipitation to other low-latitude regions sampled by the TRMM satellite will require estimation of the local error to determine appropriate temporal and spatial scales for consideration.

A simple, physically based model for precipitation involving a linear combination of Vp, Svp, and spatial lags of these variables is statistically significant and captures most of the major features of precipitation in the Himalaya at the 10 km scale, including the increased precipitation in large valleys and the double band of high precipitation in the central part of the Himalayan arc (Figs. 6 and 7). The statistical model might be improved by including a preferred wind direction and calculating the topographic slope into the wind rather than just the slope—the current model treats both- north and south-facing slopes equivalently. The relative success of this fairly simple model suggests that the decrease in temperature and saturation vapor pressure with height in the atmosphere and the direct forcing of air up slopes, especially at low elevations, are key controls on precipitation in the Himalaya at scales greater than ten kilometers.

However, the smaller scale (<200 km) maxima in precipitation and the east to west gradient in precipitation along the range are not captured by the statistical model (Fig. 6). This indicates that, not surprisingly, factors other than air temperature and simple upslope motion are important in creating these patterns. In particular, the overland distance that air must travel to the range varies from east to west, and monsoon dynamics, and the associated changes in temperature and humidity, may be important

in creating the east to west gradient along the arc. In the small regions with very high precipitation totals, dynamical convergence of air, the triggering of convection, and the motion of convective cells likely increase precipitation locally, in addition to the simple factors included in the statistical model.

The application of our physically based model as a predictive model over evolving topography does require some further research. The difference in the relative magnitudes of the coefficients of the statistical model for the whole region versus the subregion complicates the calibration of our physically based model for use in a predictive sense over evolving topography. An initial step may be to limit the domain considered in the statistical regression to the Himalayan arc itself to obtain parameters specific to this region. The difference between our statistical model and the measured TRMM climatology gives us some sense of the features that would be neglected if we were to model the coevolution of the precipitation pattern over developing Himalayan topography using our model (Figs. 6 and 7). It remains to be investigated as to whether these features create important feedbacks with the landscape that impact its evolution over time.

Precipitation patterns as measured by TRMM in the Himalaya vary considerably over small spatial scales, as has also been noted for the Alps and the Olympic Mountains of western Washington, USA. Spatial patterns of discharge are certainly important in determining the spatial variability in stream power and fluvial shear stress, and thus an understanding of the spatial patterns of precipitation and discharge is important for estimating spatial patterns of erosion in mountainous landscapes. In addition to the relationship between fluvial incision and erosion, glacial erosion rates are expected to increase with ice discharge (e.g., MacGregor et al., 2000; Tomkin and Braun, 2002), and hence with rates of solid precipitation. Therefore the tendency for more precipitation in certain areas is likely to result in high erosion rates in those areas independent of whether glacial or fluvial processes dominate. There may also be important local relationships between precipitation and erosion. For instance, Reiners et al. (2003) found that long-term erosion rates tracked spatial variation in twentieth-century precipitation across the Washington Cascades. If precipitation itself proves to be a useful predictor of spatial patterns of erosion, the importance of documenting the spatial pattern of precipitation in mountains becomes even more fundamental to our understanding of feedbacks between precipitation and topographic development. Measuring and modeling spatial variability in precipitation will no doubt provide interesting new insights into the continuing study of the interrelationships between erosion, climate, and tectonics.

ACKNOWLEDGMENTS

The data used in this study were acquired as part of the Tropical Rainfall Measuring Mission (TRMM). The algorithms were developed by the TRMM Science Team. The data were processed by the TRMM Science Data and Information System (TDSIS) and the TRMM office; they are archived and distributed by the Goddard Distributed Active Archive Center. TRMM is an international project jointly sponsored by the Japan National Space Development Agency (NASDA) and the U.S. National Aeronautics and Space Administration (NASA) Office of Earth Sciences. We thank Courtney Shumacher for help and advice on obtaining and understanding the TRMM satellite data, Robert Meneghini for information and advice on TRMM and ground clutter, Harvey Greenberg for savvy data processing and graphics, and Ana Barros and Ronald Smith for constructive critiques of the manuscript. This study was partially funded by the National Science Foundation Continental Dynamics Program grant no. 003561.

REFERENCES CITED

Anders, A.M., Roe, G.H., Durran, D.R., Montgomery, D.R., and Hallet, B., 2004, Precipitation and the form of mountain ranges: Bulletin of the American Meteorological Society, v. 85, p. 498–499.

Anselin, L., 1993, Discrete space autoregressive models, *in* Goodchild, M.F., Parks, B.O., and Steyaert, L.T., eds., Environmental modeling with GIS: New York, Oxford University Press, p. 454–469.

Barros, A.P., and Lang, T.J., 2003, Monitoring the monsoon in the Himalayas: Observations in central Nepal, June 2001: Monthly Weather Review, v. 131, p. 1408–1427, doi: 10.1175/1520-0493(2003)131<1408:MTMITH>2.0.CO;2.

Barros, A.P., and Lettenmaier, D.P., 1993, Dynamic modeling of the spatial distribution of precipitation in remote mountainous areas: Monthly Weather Review, v. 121, p. 1195–1214, doi: 10.1175/1520-0493(1993)1212.0.CO;2.

Barros, A.P., and Lettenmaier, D.P., 1994, Dynamic modeling of orographically induced precipitation: Reviews of Geophysics, v. 32, p. 265–284, doi: 10.1029/94RG00625.

Barros, A.P., Joshi, M., Putkonen, J., and Burbank, D.W., 2000, A study of the 1999 monsoon rainfall in a mountainous region in central Nepal using TRMM products and rain gauge observations: Geophysical Research Letters, v. 27, p. 3683–3686, doi: 10.1029/2000GL011827.

Barros, A.P., Kim, G., Williams, E., and Nesbitt, S.W., 2004, Probing orographic controls in the Himalayas during the monsoon using satellite imagery: Naturals Hazards and Earth System Science, v. 4, p. 29–51.

Beaumont, C., Fullsack, P., and Hamilton, J., 1992, Erosional control of active compressional orogens, *in* McClay, K.R., ed., Thrust tectonics: New York, Chapman and Hall, p. 1–18.

Bell, T.L., 1987, A space-time stochastic model of rainfall for satellite remote sensing studies: Journal of Geophysical Research, v. 92, p. 9631–9644.

Bell, T.L., and Kundu, P.N., 2000, Dependence of satellite sampling error on monthly averaged rain rates: Comparison of simple models and recent studies: Journal of Climate, v. 13, p. 449–462, doi: 10.1175/1520-0442(2000)013<0449:DOSSEO>2.0.CO;2.

Colle, B.A., Westrick, K.J., and Mass, C.F., 1999, Evaluation of the MM5 and Eta-10 precipitation forecasts over the Pacific Northwest during the cool season: Weather and Forecasting, v. 14, p. 137–154.

Daly, C., Gibson, W.P., Taylor, G.H., Johnson, G.L., and Pasteris, P., 2002, A knowledge-based approach to the statistical mapping of climate: Climate Research, v. 22, p. 99–113.

Dhar, O.N., and Rakhecha, P.R., 1981, The effect of elevation on monsoon rainfall distribution in the central Himalayas, *in* Lighthill, J., and Pearce, R.P., eds., Monsoon dynamics: New York, Cambridge University Press, p. 253–260.

Dingman, S.L., 2002, Physical hydrology: Upper Saddle River, New Jersey, Prentice Hall, 646 p.

Durran, D.R., 1986, Mountain waves, *in* Ray, P.S., ed., Mesoscale meteorology and forecasting: Boston, American Meteorological Society, p. 472–492.

Emanuel, K.A., 1994, Atmospheric convection: New York, Oxford University Press, 580 p.

Finlayson, D.P., and Montgomery, D.R., 2003, Modeling large-scale fluvial erosion in geographic information systems: Geomorphology, v. 53, p. 147–164, doi: 10.1016/S0169-555X(02)00351-3.

Finlayson, D.P., Montgomery, D.R., and Hallet, B., 2002, Spatial co-incidence of erosional and metamorphic hot spots in the Himalaya: Geol-

ogy, v. 30, p. 219–222, doi: 10.1130/0091-7613(2002)030<0219:SCORIE>2.0.CO;2.

Frei, C., and Schär, C., 1998, A precipitation climatology of the Alps from high-resolution rain-gauge observations: International Journal of Climatology, v. 18, p. 873–900, doi: 10.1002/(SICI)1097-0088(19980630)18:83.0.CO;2-9.

Groisman, P.V., and Legates, D.R., 1994, The accuracy of United States precipitation data: Bulletin of the American Meteorological Society, v. 75, p. 215–227, doi: 10.1175/1520-0477(1994)075<0215:TAOUSP>2.0.CO;2.

Hoffman, P.F., and Grotzinger, J.P., 1993, Orographic precipitation, erosional unloading, and tectonic style: Geology, v. 21, p. 195–198, doi: 10.1130/0091-7613(1993)021<0195:OPEUAT>2.3.CO;2.

Houze, R.A., 1993, Cloud dynamics: Boston, Academic Press, 573 p.

Koons, 1989, The topographic evolution of collisional mountain belts: A numerical look at the Southern Alps, New Zealand: American Journal of Science, v. 289, p. 1041–1069.

Kozu, T., Kawanishi, T., Kuroiwa, H., Kojima, M., Oikawa, K., Kumagai, H., Okamoto, K., Okumua, M., Nakatsuka, H., and Nizhikawa, K., 2001, Development of precipitation radar onboard the Tropical Rainfall Measuring Mission (TRMM) satellite: IEEE Transactions on Geoscience and Remote Sensing, v. 39, p. 102–116.

Lang, T.J., and Barros, A.P., 2002, An investigation of the onsets of the 1999 and 2000 monsoons in central Nepal: Monthly Weather Review, v. 130, p. 1299–1316, doi: 10.1175/1520-0493(2002)130<1299:AIOTOO>2.0.CO;2.

Lang, T.J., and Barros, A.P., 2004, Winter storms in the central Himalayas: Journal of the Japanese Meteorological Society, v. 82, p. 829–844, doi: 10.2151/jmsj.2004.829.

Leemans, R., and Cramer, W.P., 1991, The IIASA database for mean monthly values of temperature, precipitation and cloudiness of a global terrestrial grid: Laxenburg, Austria, International Institute for Applied Systems Analysis Publication RR-91-18, 62 p.

MacGregor, K.R., Anderson, R.S., Anderson, S.P., and Waddington, E.D., 2000, Numerical simulations of glacial-valley longitudinal profile evolution: Geology, v. 28, p. 1031–1034, doi: 10.1130/0091-7613(2000)028<1031:NSOGLP>2.3.CO;2.

Meneghini, R., Iguchi, T., Kozu, T., Liao, L., Okamoto, K., Jones, J.A., and Kwiatkowski, J., 2000, Use of the surface reference technique for path attenuation estimates from the TRMM precipitation radar: Journal of Applied Meteorology, v. 39, p. 2053–2070.

Montgomery, D.R., Balco, G., and Willett, S.D., 2001, Climate, tectonics and the morphology of the Andes: Geology, v. 29, p. 579–582, doi: 10.1130/0091-7613(2001)029<0579:CTATMO>2.0.CO;2.

Pace, R.K., and Barry, R., 1999, Spatial statistics toolbox 1.1 for Matlab: www.spatial-statistics.com (August 2003).

Reiners, P.W., Ehlers, T.A., Mitchell, S.G., and Montgomery, D.R., 2003, Coupled spatial variations in precipitation and long-term erosion rates across the Washington Cascades: Nature, v. 426, p. 645–647, doi: 10.1038/nature02111.

Roe, G.H., Montgomery, D.R., and Hallet, B., 2002, Effects of orographic precipitation variations on the concavity of steady-state river profiles: Geology, v. 30, p. 143–146, doi: 10.1130/0091-7613(2002)030<0143:EOOPVO>2.0.CO;2.

Roe, G.H., Montgomery, D.R., and Hallet, B., 2003, Orographic climate feedbacks and the relief of mountain ranges: Journal of Geophysical Research, v. 108, doi: 10.1029/2001JB001521.

Shin, K., and North, G.R., 1988, Sampling error study for rainfall estimate by satellite using a stochastic model: Journal of Applied Meteorology, v. 27, p. 1218–1231, doi: 10.1175/1520-0450(1988)027<1218:SESFRE>2.0.CO;2.

Shrestha, M.L., 2000, Interannual variation of summer monsoon rainfall over Nepal and its relation to Southern Oscillation Index: Meteorology and Atmospheric Physics, v. 75, p. 21–28, doi: 10.1007/s007030070012.

Simpson, J.E., 1987, Gravity currents in the environment and laboratory: New York, John Wiley and Sons, 244 p.

Sinclair, M.R., Wratt, D.S., Henderson, R.D., and Gray, W.R., 1997, Factors affecting the distribution and spillover of precipitation in the Southern Alps of New Zealand—A case study: Journal of Applied Meteorology, v. 36, p. 428–442, doi: 10.1175/1520-0450(1997)036<0428:FATDAS>2.0.CO;2.

Singh, P., Ramasastri, K.S., and Kumar, N., 1995, Topographical influence on precipitation distribution in different ranges of Western Himalayas: Nordic Hydrology, v. 26, p. 259–284.

Smith, R.B., 1979, The influence of mountains on the atmosphere: Advances in Geophysics, v. 21, p. 87–233.

Tomkin, J.H., and Braun, J., 2002, The influence of alpine glaciation on the relief of tectonically active mountain belts: American Journal of Science, v. 302, p. 169–190.

Tripoli, G.J., and Cotton, W.R., 1989, Numerical study of an observed orogenic mesoscale convective system: Monthly Weather Review, v. 117, p. 273–328, doi: 10.1175/1520-0493(1989)117<0273:NSOAOO>2.0.CO;2.

Willett, S.D., 1999, Orogeny and orography: The effects of erosion on mountain belts: Journal of Geophysical Research, v. 104, p. 28,957–28,981, doi: 10.1029/1999JB900248.

Manuscript Accepted by the Society 23 June 2005